Title	Planar semiconductor membranes with brightness enhanced embedded quantum dots via electron beam induced deposition of 3D nanostructures: Implications for solid state lighting
Authors	Varo, Simone;Li, Xin;Juska, Gediminas;Ranjbar Jahromi, Iman;Gocalińska, Agnieszka M.;Di Falco, Andrea;Pelucchi, Emanuele
Publication date	2020-12-11
Original Citation	Varo, S., Li, X., Juska, G., Ranjbar Jahromi, I., Gocalinska, A. M., Di Falco, A. and Pelucchi, E. (2020) 'Planar semiconductor membranes with brightness enhanced embedded quantum dots via electron beam induced deposition of 3D nanostructures: Implications for solid state lighting', ACS Applied Nano Materials, 3(12), pp. 12401-12407. doi: 10.1021/acsanm.0c02969
Type of publication	Article (peer-reviewed)
Link to publisher's version	https://doi.org/10.17630/a4f40732-16ae-47a6-9cc1-7215d962726a - 10.1021/acsanm.0c02969
Rights	© 2020, American Chemical Society. This document is the Accepted Manuscript version of a Published Work that appeared in final form in ACS Applied Nano Materials, after technical editing by the publisher. To access the final edited and published work see https://doi.org/10.1021/acsanm.0c02969
Download date	2025-04-20 04:35:43
Item downloaded from	https://hdl.handle.net/10468/10955

Planar Semiconductor Membranes with Brightness-enhanced Embedded Quantum Dots via Electron Beam Induced Deposition of 3D Nanostructures: Implications for Solid State Lighting

*Simone Varo[1] *‡, Xin Li[2]‡, Gediminas Juska[1], Iman Ranjbar Jahromi[1], Agnieszka M. Gocalinska[1], Andrea Di Falco[2] and Emanuele Pelucchi[1]*

1 Tyndall National Institute, University College Cork, Dyke Parade, Cork, T12R5CP, Republic of Ireland

2 SUPA, University of St. Andrews, School of Physics & Astronomy, Physical Science Building, North Haugh, St Andrews, KY16 9SS, United Kingdom

* simone.varo@tyndall.ie

KEYWORDS: Quantum dots, Electron Beam Induced Deposition, Microlenses, Additive Manufacturing, Photonic trimming.

ABSTRACT

The engineering of the surrounding photonic environment is one of the most successful approaches routinely used to increase light extraction efficiency and tune the properties of solid state sources of quantum light. However, results achieved so far have been hampered by the lack of a technology that allows for the straightforward fabrication of large scale 3D nano- and microfeatures, with very high resolution and sufficient flexibility in terms of available materials. In this paper we show that Electron Beam Induced Deposition can be a very promising approach to solve this issue, as exemplified by the fabrication of Pt and SiO_2 nanofeatures on a membrane containing ordered arrays of site-controlled pyramidal quantum dots. Micro-photoluminescence has been used to compare the emission of the dots before and after the deposition of the structures, remarkably showing both a significant increase in the light extraction efficiency and no degradation of the spectral quality, implying that negligible damage has been caused to the emitter due to the deposition process. This paves the way for novel post-growth processing strategies for epitaxial quantum dots used in both quantum information technologies and lighting applications.

Introduction

Epitaxially grown semiconductor quantum dots (QDs) have emerged over the last decade as extremely promising sources of non-classical light[1] due to their high quantum yield, single photon

purity and indistinguishability[2], capability of emitting entangled photons via the biexciton-exciton recombination cascade[3] and possibility to achieve electrical pumping[4,5].

However, the high refractive index of the semiconductor host matrix usually severely limits the brightness of the source due to total internal reflection, making it incompatible with any of the envisioned practical applications[6]. Moreover, the combined requirement to engineer both the properties of the emitter[7] and its interface with the surrounding photonic circuitry[8] call for sophisticated fabrication approaches: major milestones have been achieved by the community by embedding QDs within micropillar cavities[9,10,11], 2D photonic crystals[2], photonic nanowires[12], circular Bragg gratings[13], nanotrumpets[14], and by fabrication of site-controlled microlenses[15,16] on top of the semiconductor matrix. All of these approaches are usually based on multi-step processes that require locating a QD using micro photoluminescence[17,18] or cathodoluminescence[15], the definition of alignment marks and the top-down fabrication of the photonic nanostructures via electron beam lithography: the change of the exposure dose, as its customary in greyscale lithography, can allow for the fabrication of simple 3D features such as microlenses, while multi-photon optical lithographic techniques can create much more complex structures, but at the price of a lower resolution.

It is clear that the limits of the techniques employed so far have prevented the fabrication of arbitrary 3D micro- and nanostructures in the proximity of QDs, and new approaches will have to be considered to overcome the current technological barriers.

In striking contrast with conventional electron beam lithography (EBL), Electron Beam Induced Deposition[19–21] (EBID) is not based on the exposure and development of an electron-sensitive resist, but is an additive technique that uses a focused electron beam to promote the decomposition of chemical precursors inserted in the gas phase within the electron microscope chamber. By

means of 3D scanning of the electron beam, EBID allows for the local deposition of a target material and the fabrication of complex nanofeatures while retaining the typical resolution of EBL[22,23], with the additional benefit of a remarkable flexibility in terms of material choice: both oxides, such as SiO_2, as well as metals, such as Pt[24] and Au[25], can be deposited in a single processing run by interchanging gases. This paves the way for a direct deposition of hard masks to be used in subsequent dry etching steps, or of plasmonic[26] and dielectric nanostructures aimed at improving light extraction efficiency[27] and/or tailoring of the emitters properties[28].

Here we carry out a study on the possible applications of the EBID technique for the most widely used starting configuration of an epitaxial quantum dot sample, that is, a planar semiconductor membrane with embedded quantum dots.

Sample fabrication

Throughout our work we have used arrays of site-controlled pyramidal quantum dots[29,30] which can be easily located using a standard scanning electron microscope (SEM). However, it should be noted that the obtained results can be readily extended to self-assembled, and randomly distributed, Stranski-Krastanov QDs, e.g. by employing the consolidated alignment marks fabrication approach[13].

All depositions have been carried out on a sample of InGaAs in GaAs pyramidal quantum dots, grown via Metal Organic Vapor Phase Epitaxy (MOVPE) using an Aixtron 200 reactor on a (111)B GaAs substrate, patterned with inverted tetrahedra using conventional lithography and wet etching in Br:MeOH. The different decomposition kinetics of the precursors in the MOVPE reactor ensures that growth takes place preferentially on the three exposed (111)A GaAs faces of the inverted tetrahedra[31], and an interplay of kinetics and diffusion of the precursors ensures the

deterministic fabrication of QDs interconnected with a series of quantum wires along the axes of the tetrahedral, if the thicknesses of the stacked layers are properly chosen.

For the sample used in this work, first a 180 nm-thick buffer layer was grown at a temperature of 770 ℃, in order to increase the distance of the nanostructures of interest from the three exposed (111)A faces that were subjected to chemical etch, then a 75 nm AlAs layer was grown in order to facilitate the location of the quantum dots in the SEM due to the high contrast with GaAs. Finally, a series of three stacked $In_{0.25}Ga_{0.75}As$ quantum dots was grown at a lower temperature of 730 ℃ : the first two, grown with a nominal thickness of 0.4 nm, help stabilizing the environment by trapping charges generated during optical pumping along with the quantum wires that are fabricated with them, while the last one is the target QD, and is grown with a nominal thickness of 0.65 nm to ensure that its emission spectrum does not overlap with the other ones and will be the dot we will be referring to from now on.

While the epitaxial growth takes place almost exclusively inside the lithographically-defined inverted tetrahedra, the post-growth sample still retains a vestigial recess: in order to move back to the typical geometry used by the epitaxial QD community that is, a planar sample, a chemo-mechanical planarization has been carried out[32] using a 70 nm silica nanoparticle slurry (Ultra-Sol 2EX, Eminess Technologies) on a Logitech PM5 polishing machine. This ensures that the resulting surface is both flat and polished to an acceptable optical quality, with the QDs lying around 100 nm below the surface.

The sample was then placed in a Raith E-line plus EBL system for the fabrication of the nanostructures. In order to investigate the possible applications of the technique in terms of both depositable material and shapes, two series of features were fabricated above a series of QDs in this first deposition run: Pt-containing features were made by inserting the precursor

(Me_3)MeCpPt in the chamber, and decomposing it with a deposition current of 150 pA, accelerating voltage of 3 kV, dose of 1 C/cm^2, step size of 20 nm, and dwelling time of 50ms, with the sample nominally at room temperature, which is expected to lead to a Pt percentage of 30% in the final material[24], the rest being made up mostly by carbon. Secondly, SiO_2 based structures were fabricated by decomposing the precursor Penta Methyl Cyclo Penta Siloxane (PMCPS), with a deposition current of 150 pA, accelerating voltage of 3 kV, dose of 1 C/cm^2, step size of 10 nm, and dwelling time of 0.01ms with variable (100-5000) writing loops, again at room temperature. Chemical analysis performed using EDX spectroscopy with a Quanta 650 SEM shows the amount of carbon incorporated in the structures to be surprisingly very low and not detectable with the tool employed. A high purity of the material is however in line with what previously reported using similar deposition conditions[33]. Typical EDX spectra are reported in the Supplementary Materials on Table S2 for the reader's convenience.

A summary of the fabrication procedure employed is reported in figure 1.

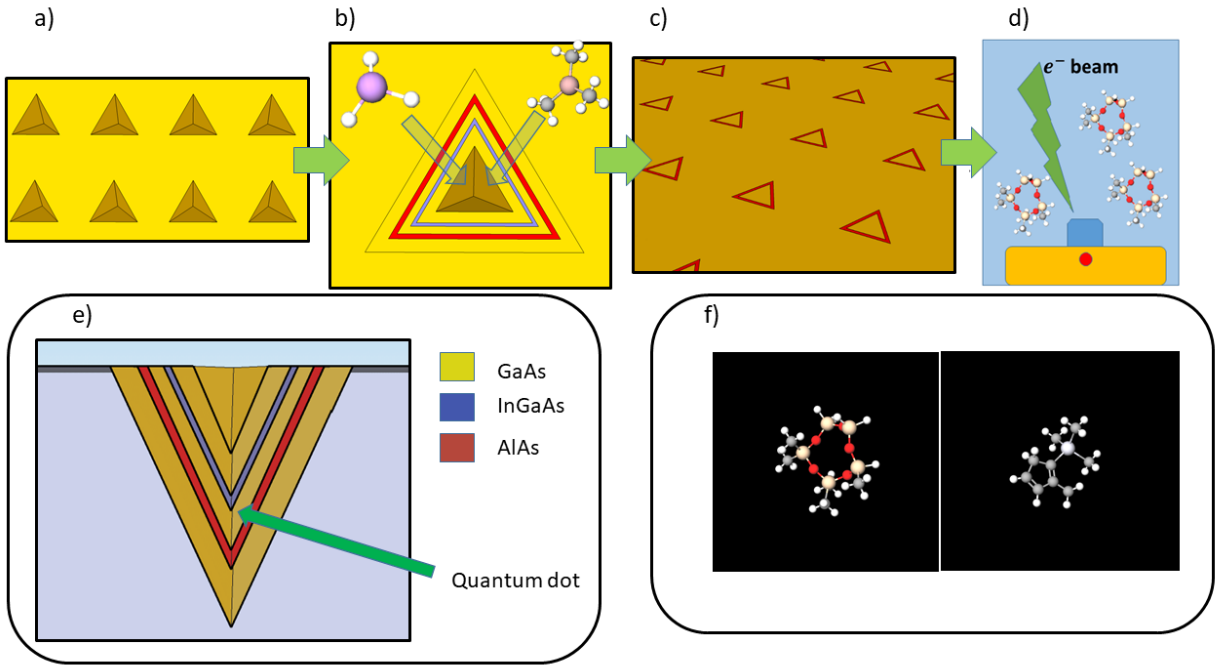

Figure 1 Representation of the steps in the fabrication of the samples: a) patterning of the substrate; b) MOVPE growth, organometallic precursors dissociate preferentially on the three exposed 111A faces; c) planarization; d) EBID growth; e) cross section of the structure after MOVPE growth. The QD is formed by enclosing a thing InGaAs layer between two GaAs barriers. f) EBID precursors PMCPS (left) and $(Me_3)MeCpPt$ (right)

A wide array of shapes, ranging from nanopillar-like adiabatically tapered waveguides to microlenses was fabricated by exploiting the 3-dimensional capabilities of the technique and in order to investigate their effects on the underlying QD. Images of each of the fabricated structures are reported in the Supplementary Materials as well (figures S1-S5), while some significant ones are included in figure 2 as reference.

Pt alignment marks were also fabricated to allow for an easier location and identification of the processed QDs in the subsequent micro photoluminescence (μ-PL) measurement stages: these were carried out using a confocal setup and a helium closed-cycle cryostat that cooled the sample to a temperature of 8 K. All measurements at this stage were performed under non-resonant continuous wave excitation conditions with a 635 nm wavelength laser using a 0.45 numerical aperture objective (Mitutoyo) for light collection, with an excitation power density of 150 $nW/\mu m^2$ for all the structures.

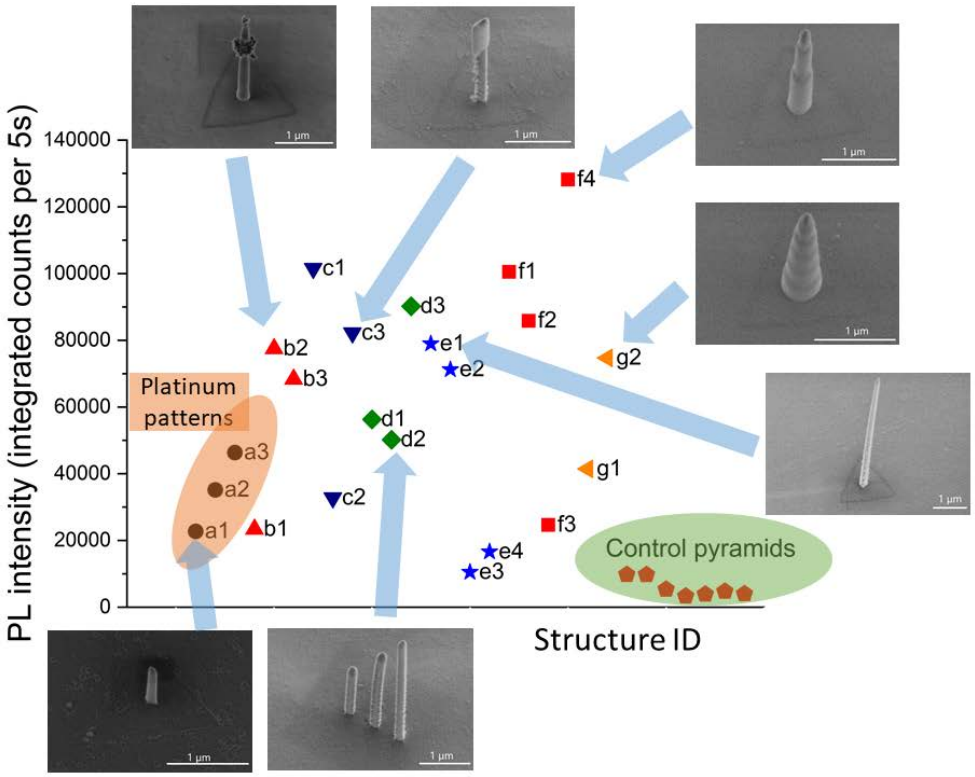

Figure 2. Integrated CCD counts for the QDs after the fabrication of nanostructures on top. Control QDs (without any deposited structure) are also shown for comparison. Insets display some fabricated nanofeatures.

Results and discussion

As can be seen from figure 2, nearly every of the fabricated structures provide a boost of the extraction efficiency when compared to the control (unprocessed) QDs.

For the three Pt-based nanopillars, (left low corner in Fig. 2), it is worth mentioning no significant change in the lifetime was detected, meaning that a plasmonic coupling between the quantum emitter and the deposited structure can be ruled out: this is likely due to the latter's relatively small Pt content (around 30% with the used deposition parameters), resonance

frequency, as well as the distance of the buried QD from the surface that prevents efficient overlapping of the QD's dipole with the mode sustained by the antenna. As plasmonic effects have already been achieved using the same deposition technique[28], we believe that this unsatisfactory performance can be mostly ascribed to the planarization technique hereby employed, that provides limited control over the dot's final distance from the surface.

Dielectric micro- and nano-features on the other hand have shown remarkable results, with values of the light extraction efficiency often surpassing the ones obtained from pyramidal quantum dots using the conventional back-etching technique (i.e. the conventional approach to obtain apex-up pyramids and improve extraction efficiency[34]). These structures work by changing the dielectric environment above the semiconductor, reducing internal reflection and displaying a waveguiding effect (more pronounced for the pillar-like ones) that helps not only extracting photons from the surface of the high refractive index GaAs, but also collecting it with the objective by reducing the angular distribution of the emitted light.

These results, while already proving the capabilities of this technique, can hardly be used to reach any general conclusion on the properties of each of the deposited structures as they do not take into account the differences in term of blinking and quantum yield of the QDs they were fabricated onto. Moreover, the structures themselves, by channeling and focusing light in different ways, are expected to affect the excitation efficiency of the QD lying beneath it, thus making the use of the same excitation power a rather naïve approach for a systematic comparison.

In order to address these shortcomings, we have exploited the previously deposited alignment marks to carry out the mapping of a series of 30 quantum dots, that were subsequently used for a second run of depositions (Figure 3): this ensured that we were able to quantitatively estimate the effect of the structures in terms of both light extraction efficiency and changes of the spectra due

to defects or strain created by the deposition itself by comparing the measurements taken prior and after the in-situ fabrication had been carried out. Additional care was employed to avoid deposition nonuniformities by simplifying the geometry of the structures, which are now simple cones of different base radii and heights. Geometrical parameters were also varied smoothly between the structures in order to both investigate the presence of trends in the PL enhancement and assess the reproducibility of the results via comparison of similar structures.To circumvent the aforementioned problem of different excitation efficiencies with and without the structures, during the measurements of the second set of depositions, every QD has been excited close to the saturation level of ground state-related transitions: the resulting photoluminescence spectra was composed of several excitonic complexes, the dominant ones typically being neutral exciton, biexciton, negative and positive trions, excited positive trion and positively charged biexcitons. Ideally, an identical or very similar spectral shape was recreated in every case from the corresponding QDs after the deposition of the nanostructures, indicating the same QD population conditions. Light extraction enhancement was subsequently calculated as a ratio of an integrated QD photoluminescence signal post- and prior-deposition. This technique also allowed for the overcoming of uncertainties arising due to variations in the experimental conditions, such as a different focal distance and excitation power.

Furthermore, having already proven the flexibility of the technique in terms of material choices, we have decided to narrow down the scope of our investigation to a subset of the previously investigated geometries: we have thus deposited a series of extruded SiO_2 structures whose shapes range from dome-like to conical to pillar-like, in order to determine the effect of different base radiuses and heights. Details and images of each of the fabricated structures are once more included as Supplementary Materials (figures S6-S10) for the reader’s convenience.

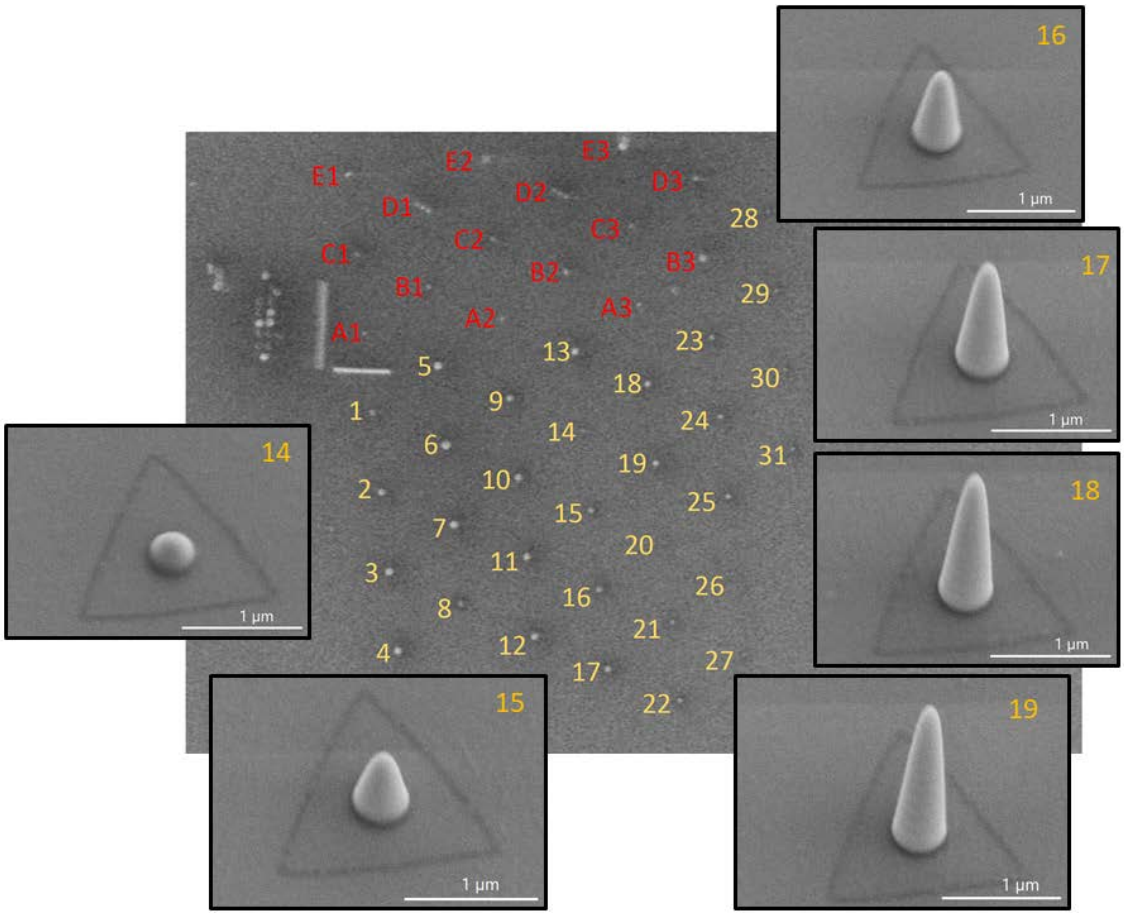

Figure 3. Mapping of the sites used for the fabrication of structures above the QDs and numbers identifying the single structures. The insets show some examples of the deposited structures. Alignment marks can be seen in the top left corner.

First of all, a comparison of the measurements performed before and after the deposition (figure 4) shows surprisingly negligible changes in the dominant spectral features, a telltale sign that the deposition technique does not, in fact, cause significant damage to the quantum dots or to the matrix they are embedded into. Minor spectral shifts, usually in the order of tens of µeV, can be attributed to either small strains field induced by the structures or to local temperature variations

caused by the different heat distribution and dissipation in close proximity of the QD once the thermally insulating dielectric is deposited.

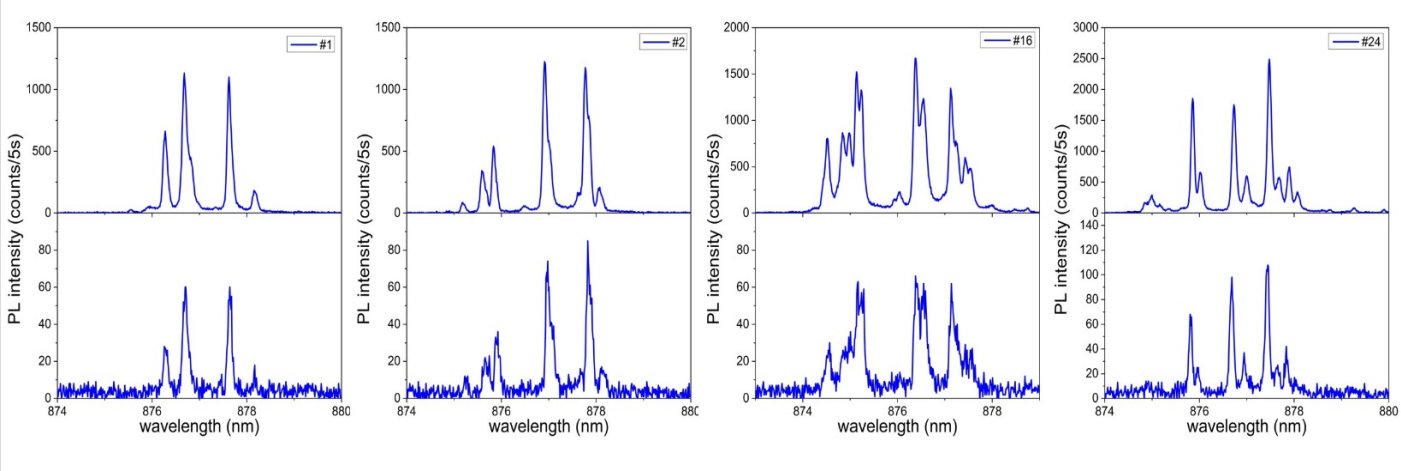

Figure 4. Comparison of the spectra before (bottom) and after (top) the fabrication of the structures for four randomly chosen QDs, showing negligible spectral shifts and excitonic distribution.

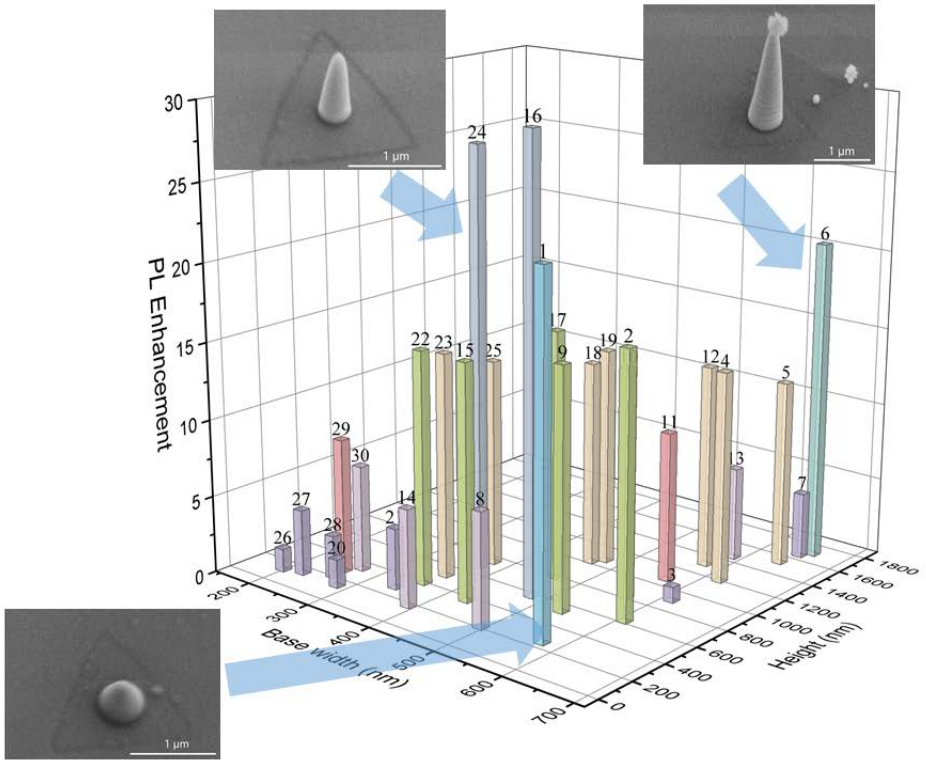

Figure 5. Enhancement of the brightness for the 30 deposited dielectric nanostructures with different heights and base widths. Numbers on top of the bars identify the corresponding structure, whereas the three insets show the shape of the brightest ones

The brightness of the sources is clearly increased significantly after the deposition, up to an order of magnitude or more as can be seen in figure 5, which summarizes the key finding of our investigation. However, the interpretation of the obtained results is not straightforward: first of all, it can be noticed that in comparison to the dome-like, low-height structures, the elongated, tapered features often provide a far more significant boost of the light extraction efficiency (LEE). Different mechanisms are likely simultaneously at play and their relative effects difficult to decouple from each other: it is intuitive that a larger base radius should allow the microstructure to collect and channel more light that would otherwise be trapped inside the semiconductor due to total internal reflection. Secondly, the shape of the microstructure affects, via Fresnel reflection at the interface and adiabatic coupling, the amount of light that leaves it, as well as the far field of the radiated light, and thus the final collection efficiency from the objective.

For the low-height, dome-like structures, it is apparent that the LEE depends more on their base size than on their aspect ratio, as one would intuitively assume due to their behavior being similar to that of lenses: in this regard, it comes to no surprise that structure number 1, having the largest base radius, provides by far the best performance, and one of the best performances overall. Similar structures such as number 14 and 18 however display a far less significant enhancement, due to their base radiuses being smaller and thus collecting less light from the quantum emitter, despite being closer in shape to a hemispherical lens. Minor displacements from the shape of an ideal

micro-lens, implying that the light is emitted in a broader cone, are likely to be counterbalanced by the high numerical aperture of the objective.

It is interesting to observe that the remaining, tapered, pillar-like structures display boosts of the LEE that look relatively constant across a broad set of geometrical parameters, as clearly seen in figure 4, showing remarkably coarse fabrication tolerances, albeit only two of them, number 16 and 24, manage to break the level reached by the best dielectric lens (number 1). Moreover, they usually perform better than the dome-like structures of similar base radius: this is clear when comparing for instance structures 14 and 22 or 23, and can probably be ascribed to their ability to efficiently couple light that propagates along their axes in the free space via their adiabatic tapering, as it happens with semiconductor nanopillars[35]. Surprisingly, however, structures with a larger base radius and very small aspect ratio (and thus very small tapering angle), such as number 7 or 13, actually perform worse than those with a smaller base, and a larger tapering angle.

Structure number 6, that displayed a far more significant boost of the LEE when compared to the relatively similar structures numbered 5 and 7, was affected by some fabrication imperfections (figure 4) that are likely to cause a scattering of the light from the tip.This might suggest that the quality of the latter plays a more fundamental role in determining the performance of these kind of structures than other geometrical parameters.

FDTD simulations

In order to better understand the effect of geometrical parameters and assess the impact of the purity of the deposited material on the performance of EBID-fabricated structures, an extensive simulation work has been performed using Lumerical FDTD.

In all of our simulations we have assumed the dielectric structure to be conical in shape, and independently varied its base radius and its height to define a matrix of 15x15 simulations.

For each of said simulations, the collection efficiency by a 0.45 NA objective like the one employed in our experiment was estimated via integration of the far field, and the collection enhancement with respect to the bare GaAs substrate was calculated by taking the ratio of the former to collection efficiency of the latter case.

Furthermore, we computed the aforementioned matrix 3 times, assuming on each run a different refractive index for the dielectric in order to evaluate the impact of carbon impurities: to do so, we estimated the refractive index to be the weighted average of that of SiO_2 and graphite, with concentrations of the latter being of 0, 15 and 30 % for each of the three runs. It should be noted however that this only provides a very rough estimation of the effects of Carbon incorporation in the structure, as the latter will likely be bound in Si-O-C complex whose optical behavior might differ significantly from the one we are assuming, besides the fact that we are neglecting any porosity in the material, which will reduce the refractive index. Regardless of our naïve assumption on the relation between refractive index and stoichiometry of the deposited nanomaterial, our results allow to draw some general conclusions on the performance of the fabricated nanostructures with respect to variations of their refractive index.

First of all, by comparing the graphs displayed in figure 6, it can be easily seen that pure silica structures exhibit the best performance, while the presence of carbon degrades their effectiveness. Taller structures in this case tend to extract less light, with the LEE reaching a plateau and then decreasing, a behavior we ascribe to absorption losses incurred during the propagation through the structure itself: as the imaginary part of the refractive index increases, the maximum of the predicted LEE both lowers and progressively shifts to shorter structures.

This remarks that a control of the purity of the deposited material is of paramount importance for further photonic applications.

For the pure silica batch of simulations a plateau is not reached for the investigated geometries: we believe that similarly to what happens with semiconductor nanowires[36], the tapering angle of the structure plays a key role in determining the amount of light which is collected by the objective. As the cone behaves as an adiabatic taper, an increment in the radius of the base will indeed increase the amount of light funneled into the dielectric structure, but the fraction which is ultimately collected will drop if the height of the structure is not increased accordingly. These results agree qualitatively with the ones of our experimental investigation reported in figure 5, where a similar trend is displayed, and imply that the base radius and height of the structures cannot be treated as independent parameters for a maximization of the LEE.

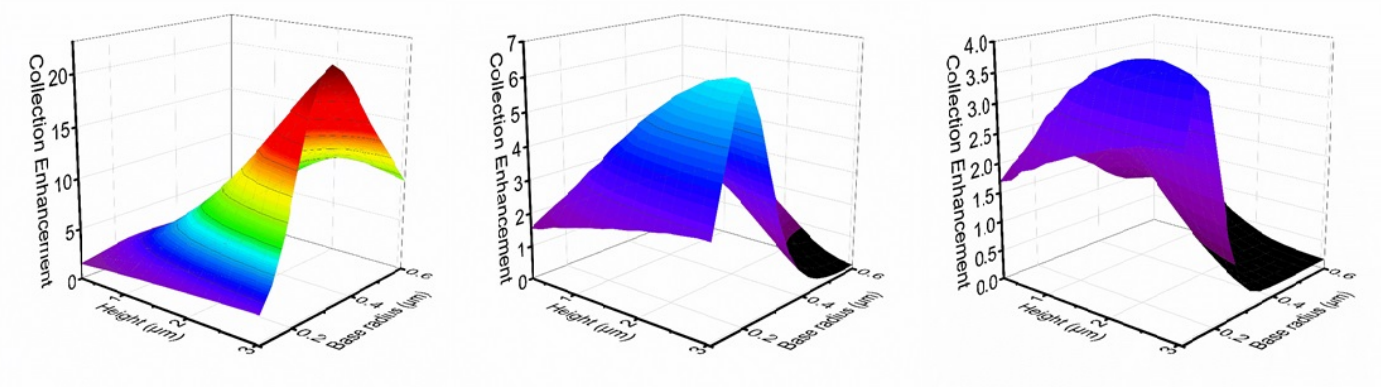

Figure 6 Simulated enhancement of PL collection efficiency for structures with different sizes and carbon content. From left to right, C incorporation of 0, 15 and 30 %

Conclusions

In this preliminary investigation, we have shown for the first time that the EBID technique can be a useful resource for the post-growth processing of epitaxial quantum dots, by significantly enhancing light extraction from the semiconductor matrix without causing any degradation in the quality of the dot and its emission features.

While the overall extraction efficiency hereby achieved by means of the fabricated nanostructures is definitely below the levels reached by the best performing semiconductor photonic cavities, the results are promising, especially in view of the possibility of using the deposited dielectric in subsequent processing steps as a hard mask for dry etching: this would allow for instance to fabricate tapered[35], or lens-topped, semiconductor nanowires with unprecedented precision.

More broadly, we believe that the 3D capabilities of the technique, coupled to its flexibility in terms of material choices, make it extremely attractive to the semiconductor quantum dot community, where extensive and complex nanofabrication is often performed on individual quantum emitters: for this purpose, the lack of damages induced in the processed QDs, as reported in our work, is of the utmost importance.

From the direct deposition of dielectric masks for dry etching and metal contacts for electrical nanodevices, to the fabrication of complex structures on top of the semiconductors to improve light extraction or engineer the projected far field, we expect EBID to play a significant role in the years to come in the field of quantum photonics with semiconductor QDs.

ASSOCIATED CONTENT

The following files are available free of charge.

Supporting information (PDF): Details and high resolution SEM images of each of the fabricated structures, and EDX analysis

AUTHOR INFORMATION

Corresponding Author

*Simone Varo, Tyndall National Institute, Dyke Parade, Cork, Republic of Ireland. simone.varo@tyndall.ie

Author Contributions

The manuscript was written through contributions of all authors. All authors have given approval to the final version of the manuscript. ‡These authors contributed equally.

Funding Sources

This research was supported by Science Foundation Ireland under Grant Nos. 15/IA/2864, and 12/RC/2276_P2. ADF acknowledges support from EPSRC (EP/L017008/1) and ERC (Grant No. 819346).

Notes

Any additional relevant notes should be placed here.

ACKNOWLEDGMENT

The authors are grateful to Dr. K. Thomas for the MOVPE system support.

ABBREVIATIONS

MOVPE, Metal-Organic Vapor Phase Epitaxy; EBID, Electron beam Induced Deposition; QDs, Quantum Dots; LEE, Light Extraction Efficiency

REFERENCES

(1) Shields, A. J. Semiconductor Quantum Light Sources. *Nat. Photonics* **2007**, *1* (4), 215–223.

(2) Englund, D.; Majumdar, A.; Faraon, A.; Toishi, M.; Stoltz, N.; Petroff, P.; Vučkovi, J. Resonant Excitation of a Quantum Dot Strongly Coupled to a Photonic Crystal Nanocavity. *Phys Rev. Lett.* **2010**, 104, 073904.

(3) Benson, O.; Santori, C.; Pelton, M.; Yamamoto, Y. Regulated and Entangled Photons from a Single Quantum Dot. *Phys Rev. Lett.* **2000**, *84, 2513*.

(4) Chung, T. H.; Juska, G.; Moroni, S. T.; Pescaglini, A.; Gocalinska, A.; Pelucchi, E. Selective Carrier Injection into Patterned Arrays of Pyramidal Quantum Dots for Entangled Photon Light-Emitting Diodes. *Nat. Photonics* **2016**, *10* (12), 782–787.

(5) Zhang, J.; Wildmann, J. S.; Ding, F.; Trotta, R.; Huo, Y.; Zallo, E.; Huber, D.; Rastelli, A.; Schmidt, O. G. High Yield and Ultrafast Sources of Electrically Triggered Entangled-Photon Pairs Based on Strain-Tunable Quantum Dots. *Nat. Commun.* **2015**, *6*, 1–7.

(6) Zwiller, V.; Björk, G. Improved Light Extraction from Emitters in High Refractive Index Materials Using Solid Immersion Lenses. *J. Appl. Phys.* **2002**. 92, 660-665

(7) Höfer, B.; Zhang, J.; Wildmann, J.; Zallo, E.; Trotta, R.; Ding, F.; Rastelli, A.; Schmidt, O. G. Independent Tuning of Excitonic Emission Energy and Decay Time in Single Semiconductor Quantum Dots. *Appl. Phys. Lett.* **2017**, *110* (15), 151102.

(8) Norman, J. C.; Jung, D.; Wan, Y.; Bowers, J. E. Perspective: The Future of Quantum Dot Photonic Integrated Circuits. *APL Photonics* **2018**, *3* (3), 030901.

(9) Reitzenstein, S.; Forchel, A. Quantum Dot Micropillars. *J. Phys. D Appl. Phys.* **2010**, *43* (43), 33001–33025.

(10) Somaschi, N.; Giesz, V.; De Santis, L.; Loredo, J. C.; Almeida, M. P.; Hornecker, G.; Portalupi, S. L.; Grange, T.; Antón, C.; Demory, J.; Gómez, C.; Sagnes, I.; Lanzillotti-

Kimura, N. D.; Lemaítre, A.; Auffeves, A.; White, A. G.; Lanco, L.; Senellart, P. Near-Optimal Single-Photon Sources in the Solid State. *Nat. Photonics* **2016**, *10* (5), 340–345.

(11) Michler, P.; Kiraz, A.; Becher, C.; Schoenfeld, W. V.; Petroff, P. M.; Zhang, L.; Hu, E.; Imamoğlu, A. A Quantum Dot Single-Photon Turnstile Device. *Science.* **2000**, *290* (5500), 2282–2285.

(12) Reimer, M. E.; Bulgarini, G.; Akopian, N.; Hocevar, M.; Bavinck, M. B.; Verheijen, M. A.; Bakkers, E. P. A. M.; Kouwenhoven, L. P.; Zwiller, V. Bright Single-Photon Sources in Bottom-up Tailored Nanowires. *Nat. Commun.* **2012**, *3* (1), 737.

(13) Kolatschek, S.; Hepp, S.; Sartison, M.; Jetter, M.; Michler, P.; Portalupi, S. L. Deterministic Fabrication of Circular Bragg Gratings Coupled to Single Quantum Emitters via the Combination of *in-Situ* Optical Lithography and Electron-Beam Lithography. *J. Appl. Phys.* **2019**, *125* (4), 045701.

(14) Munsch, M.; Malik, N. S.; Dupuy, E.; Delga, A.; Bleuse, J.; Gérard, J.-M.; Claudon, J.; Gregersen, N.; Mørk, J. Dielectric GaAs Antenna Ensuring an Efficient Broadband Coupling between an InAs Quantum Dot and a Gaussian Optical Beam. *Phys. Rev. Lett.* **2013**, *110* (17), 177402.

(15) Gschrey, M.; Thoma, A.; Schnauber, P.; Seifried, M.; Schmidt, R.; Wohlfeil, B.; Krüger, L.; Schulze, J. H.; Heindel, T.; Burger, S.; Schmidt, F.; Strittmatter, A.; Rodt, S.; Reitzenstein, S. Highly Indistinguishable Photons from Deterministic Quantum-Dot Microlenses Utilizing Three-Dimensional in Situ Electron-Beam Lithography. *Nat. Commun.* **2015**, *6*.

(16) Ma, Y.; Kremer, P. E.; Gerardot, B. D. Efficient Photon Extraction from a Quantum Dot in a Broad-Band Planar Cavity Antenna. *J. Appl. Phys.* **2014**, *115* (2), 023106.

(17) Sartison, M.; Portalupi, S. L.; Gissibl, T.; Jetter, M.; Giessen, H.; Michler, P. Combining In-Situ Lithography with 3D Printed Solid Immersion Lenses for Single Quantum Dot Spectroscopy. *Sci. Rep.* **2017**, *7* (1), 39916.

(18) Sapienza, L.; Davanço, M.; Badolato, A.; Srinivasan, K. Nanoscale Optical Positioning of Single Quantum Dots for Bright and Pure Single-Photon Emission. *Nat. Commun.* **2015**, *6* (1), 7833.

(19) Huth, M.; Porrati, F.; Schwalb, C.; Winhold, M.; Sachser, R.; Dukic, M.; Adams, J.; Fantner, G. Focused Electron Beam Induced Deposition: A Perspective. *Beilstein J. Nanotechnol.* **2012**, *3* (1), 597–619.

(20) van Dorp, W. F.; Hagen, C. W. A Critical Literature Review of Focused Electron Beam Induced Deposition. *J. Appl. Phys.* **2008**, *104* (8), 081301.

(21) De Angelis, F.; Liberale, C.; Coluccio, M. L.; Cojoc, G.; Di Fabrizio, E. Emerging Fabrication Techniques for 3D Nano-Structuring in Plasmonics and Single Molecule Studies. *Nanoscale* **2011**, *3* (7), 2689-2696.

(22) Fowlkes, J. D.; Winkler, R.; Lewis, B. B.; Fernández-Pacheco, A.; Skoric, L.; Sanz-Hernández, D.; Stanford, M. G.; Mutunga, E.; Rack, P. D.; Plank, H. High-Fidelity 3D-Nanoprinting via Focused Electron Beams: Computer-Aided Design (3BID). *ACS Appl. Nano Mater.* **2018**, *1* (3), 1028–1041.

(23) Jesse, S.; Borisevich, A. Y.; Fowlkes, J. D.; Lupini, A. R.; Rack, P. D.; Unocic, R. R.; Sumpter, B. G.; Kalinin, S. V.; Belianinov, A.; Ovchinnikova, O. S. Directing Matter: Toward Atomic-Scale 3D Nanofabrication. *ACS Nano.*, **2016**, pp 5600–5618.

(24) Frabboni, S.; Gazzadi, G. C.; Felisari, L.; Spessot, A. Fabrication by Electron Beam Induced Deposition and Transmission Electron Microscopic Characterization of Sub-10-Nm

Freestanding Pt Nanowires. *Appl. Phys. Lett.* **2006**, *88* (21), 213116.

(25) Shawrav, M. M.; Taus, P.; Wanzenboeck, H. D.; Schinnerl, M.; Stöger-Pollach, M.; Schwarz, S.; Steiger-Thirsfeld, A.; Bertagnolli, E. Highly Conductive and Pure Gold Nanostructures Grown by Electron Beam Induced Deposition. *Sci. Rep.* **2016**, *6* (1), 34003.

(26) Winkler, R.; Schmidt, F. P.; Haselmann, U.; Fowlkes, J. D.; Lewis, B. B.; Kothleitner, G.; Rack, P. D.; Plank, H. Direct-Write 3D Nanoprinting of Plasmonic Structures. *ACS Appl. Mater. Interfaces* **2017**, *9* (9), 8233–8240.

(27) Pfeiffer, M.; Lindfors, K.; Wolpert, C.; Atkinson, P.; Benyoucef, M.; Rastelli, A.; Schmidt, O. G.; Giessen, H.; Lippitz, M. Enhancing the Optical Excitation Efficiency of a Single Self-Assembled Quantum Dot with a Plasmonic Nanoantenna. *Nano Lett.* **2010**, *10* (11), 4555–4558.

(28) Li, X.; Su, R.-L.; Zhou, Z.-K.; Yu, Y.; Di Falco, A. Photonic Trimming of Quantum Emitters via Direct Fabrication of Metallic Nanofeatures. *APL Photonics* **2018**, *3* (7), 071301.

(29) Juska, G.; Dimastrodonato, V.; Mereni, L. O.; Gocalinska, A.; Pelucchi, E. Towards Quantum-Dot Arrays of Entangled Photon Emitters. *Nat. Photonics* **2013**, *7* (7), 527–531.

(30) Dimastrodonato, V.; Pelucchi, E.; Vvedensky, D. D. Self-Limiting Evolution of Seeded Quantum Wires and Dots on Patterned Substrates. *Phys. Rev. Lett.* **2012**, *108* (25), 256102.

(31) Pelucchi, E.; Moroni, S. T.; Dimastrodonato, V.; Vvedensky, D. D. Self-Ordered Nanostructures on Patterned Substrates. *J. Mater. Sci. Mater. Electron.* **2018**, *29* (2), 952–967.

(32) Varo, S.; Juska, G.; Ranjbar, I.; Moroni, S.; Gocalinska, A.; Pelucchi, E. Engineering Site-Controlled Quantum Dots for Optical Quantum Information Processing. In *Low-*

Dimensional Materials and Devices 2019; Kobayashi, N. P., Talin, A. A., Davydov, A. V., Eds.; SPIE, 2019; Vol. 11085, p 6.

(33) de Boer, S. K.; van Dorp, W. F.; De Hosson, J. T. M. Charging Effects during Focused Electron Beam Induced Deposition of Silicon Oxide. *J. Vac. Sci. Technol. B, Nanotechnol. Microelectron. Mater. Process. Meas. Phenom.* **2011**, *29* (6), 06FD01.

(34) Juska, G.; Murray, E.; Dimastrodonato, V.; Chung, T. H.; Moroni, S.; Gocalinska, A.; Pelucchi, E. Conditions for Entangled Photon Emission from (111)B Site-Controlled Pyramidal Quantum Dots. *J. Appl. Phys* **2015,** 117, 134302

(35) Claudon, J.; Bleuse, J.; Malik, N. S.; Bazin, M.; Jaffrennou, P.; Gregersen, N.; Sauvan, C.; Lalanne, P.; Gérard, J.-M. A Highly Efficient Single-Photon Source Based on a Quantum Dot in a Photonic Nanowire. *Nat. Photonics* **2010**, *4* (3), 174–177.

(36) Gregersen, N.; Nielsen, T. R.; Claudon, J.; Gérard, J.-M.; Mørk, J. Controlling the Emission Profile of a Nanowire with a Conical Taper. *Opt. Lett.* **2008**, *33* (15), 1693-1695.